International Journal of Computational Methods and Experimental Measurements
https://www.acadlore.com/journals/IJCMEM

# Study of the Thermal Performance and Entropy Generated by Laminar Flow of a Nanofluid in Pipes

Zohra Souad Benguerraiche[1*], Rachid Bessaïh [2]

[1] LEAP Laboratory, Department of Mechanical and Electromechanical Engineering, Abd El Hafid Boussouf University-Mila, 43000 Mila, Algeria
[2] LEAP Laboratory, Department of Mechanical Engineering, Frères Mentouri University-Constantine 1, 25000 Constantine, Algeria

[*] Correspondence: Zohra Souad Benguerraiche (z.benguerraiche@centre-univ-mila.dz)

**Received:** 08-21-2025 **Revised:** 09-21-2025 **Accepted:** 09-26-2025

**Citation:** Z. S. Benguerraiche and R. Bessaïh, "Study of the thermal performance and entropy generated by laminar flow of a nanofluid in pipes," *Int. J. Comput. Methods Exp. Meas.*, vol. 13, no. 3, pp. 709–725, 2025. https://doi.org/10.56578/ijcmem130318.



**Abstract:** This research numerically investigates entropy generation in a laminar forced convective flow of $Al_2O_3$-water nanofluid within a 2D axisymmetric pipe under uniform heat flux. The study employed aluminum oxide nanoparticles with a consistent diameter of 30nm, dispersed in water at volumetric concentrations of 1% to 4%. For Reynolds numbers (Re) ranging from 200 to 900, the analysis focused on the interplay between the Nusselt number, thermal-hydraulic performance, and entropy generation as functions of both flow velocity and nanoparticle concentration. Results show that elevating the Re and volume fraction not only increases the Nusselt number but also reduces the total entropy generation by 22.25%. A corresponding rise in pressure drop was also observed with these increases. Consequently, the application of $Al_2O_3$-water nanofluid proves to be thermodynamically advantageous, enhancing heat transfer characteristics while simultaneously suppressing entropy generation.

**Keywords:** $Al_2O_3$ nanofluid; Axisymmetric; Base fluid; Entropy generation; Forced convection

## 1 Introduction

Internal duct flow, defined as the movement of a fluid within enclosed conduits like pipes, is a fundamental and widely researched area in fluid dynamics. The defining characteristic of such flow is the presence of solid boundaries, which profoundly influences the behavior and properties of the working fluid [1–4]. Understanding these properties and the fluid's response to confinement is crucial, given its prevalence in engineering systems including power plants, air conditioning units, and heat exchangers. Consequently, a primary focus for researchers has been the accurate prediction of fluid velocity and heat transfer characteristics within these ducts [4].

The choice of working fluid is a critical factor, as it directly dictates the flow characteristics in any physical or computational model. Thermophysical properties—such as density, viscosity, and thermal conductivity—exert a significant influence on flow behavior. For example, a fluid with high viscosity resists motion, leading to slower flow rates, whereas a low-viscosity fluid flows more readily. Similarly, denser fluids generally result in higher pressure drops and slower flows, while less dense fluids facilitate lower pressure and faster velocities. To improve system performance, significant research efforts have been dedicated to developing novel working fluids with superior thermal properties compared to conventional options, as enhancing these properties directly impacts the hydrodynamic and thermal performance [5]. This pursuit led to the innovation of engineered fluids containing nanoscale particles.

These synthetic nanoparticles can be produced from various natural elements like Copper, Gold, Aluminum, and Zinc. Specifically, a nanofluid is a base fluid infused with suspended particles typically smaller than 100 nanometers. The dispersion of these particles can markedly improve the fluid's thermal conductivity, positioning nanofluids as a highly promising medium for advanced heat transfer applications [6].

The experimental investigations remain crucial for advancing nanofluid technology, as they provide the essential data on thermophysical properties needed for practical system design. The work of Vajjha and Das [7], for instance, underscores this approach by deriving empirical correlations directly from laboratory measurements of thermal

conductivity. These experimental findings are fundamentally interpreted and contextualized within the established principles of heat transfer, which are comprehensively detailed in foundational texts such as Incropera [8].

This potential for efficiency gains has attracted considerable scientific interest. A nanofluid is essentially a two-component mixture comprising a base fluid (e.g., water or oil) and nanoparticles. Studies have confirmed that the inclusion of nanoparticles enhances the thermophysical properties of the base fluid [9, 10].

An experimental investigation by Hozien et al. [1] examined the hydrothermal performance of $TiO_2$/water, Ag/water, and ZnO/water nanofluids (all at 0.25% volume fraction) flowing through helical coils under a constant wall temperature. They reported that increasing the coil pitch reduces both the pressure drop and the Nusselt number. While the nanofluids offered improved heat transfer, this benefit came with the drawback of an increased pressure drop. Lodhi et al. [2] experimentally studied the thermally developing laminar flow of $Al_2O_3$/water nanofluid in a microchannel at Reynolds numbers from 300 to 1000. Their findings indicated a friction factor increase of up to 22.7% for the nanofluid, while the heat transfer coefficient saw a maximum improvement of 24.5% at a 3% volume fraction compared to distilled water. Hussien et al. [11] explored the entropy generation and heat transfer of hybrid nanofluids based on multi-walled carbon nanotubes and graphene nanoplatelets (MWCNTs/GNPs). Their results validated standard heat transfer coefficient methodologies for microtubes and demonstrated a significant 37.5% reduction in the total entropy generation rate.

Heyhat et al. [12] conducted an experimental study on the friction factor and heat transfer coefficient for laminar nanofluid flow in a pipe, using $Al_2O_3$ nanoparticles dispersed in distilled water at volume fractions from 0.1% to 2%. They observed a higher heat transfer coefficient for nanofluids relative to the base fluid, with further enhancement at higher Reynolds numbers and particle concentrations. Hwang et al. [13] experimentally measured pressure drop and convection heat transfer coefficients for fully developed laminar $Al_2O_3$/water nanofluid flow in a circular duct. The heat transfer coefficient increased by 8% at a 0.3% volume fraction, an augmentation that could not be predicted by the established correlation from Shah and London [14] and Shah and Bhatti [15]. Anand [16] performed an analytical analysis of entropy generation for laminar nanofluid flow in a circular pipe under an isothermal boundary condition, considering both $Al_2O_3$/water and $Al_2O_3$/ethylene glycol. The study concluded that adding nanoparticles is only beneficial at lower Reynolds numbers and with low-viscosity base fluids. It was also established that the entropy generation for a pipe in a constant-temperature external fluid falls between the values for isoflux and isothermal boundary conditions.

Salman et al. [17] numerically examined forced convection in a 3D microtube with varying wall heat fluxes, testing ZnO, $SiO_2$, CuO, and $Al_2O_3$ nanofluids. Their results indicated that pure ethylene glycol had the lowest Nusselt number, followed by $Al_2O_3$/ethylene glycol and CuO/ethylene glycol, while $SiO_2$/ethylene glycol nanofluid achieved the highest. For all nanofluids, the Nusselt number improved with higher nanoparticle concentration but decreased with larger particle size. The Nusselt number was found to be unaffected by the applied heat flux. Ting and Hou [18] studied the forced convection characteristics of laminar $Al_2O_3$/water nanofluid flow in a horizontal circular pipe under an isothermal boundary condition. Using nanoparticle diameters of 40 nm and volume fractions of 0.1% to 2%, they found that the heat transfer coefficient increased with both volume fraction and Reynolds number, though this was accompanied by a higher-pressure drop. Notably, the heat transfer performance with a 2% volume concentration was augmented by 32% compared to pure water. Zhang et al. [19] computationally investigated conjugate heat transfer in microtubes, finding that axial wall heat conduction promoted a uniform heat flux at the inner wall surface. Fard et al. [20] used a computational fluid dynamics approach with single-phase models to study laminar nanofluid flow in a circular pipe under an isothermal condition. Their findings confirmed a clear increase in the heat transfer coefficient with nanoparticle concentration and showed good agreement between the single-phase model results and experimental data.

Foundational research in laminar forced convection heat transfer, such as the work of Shah and London [14] and the handbook by Shah and Bhatti [15], established essential benchmark references, though they were confined to conventional fluids without addressing the characteristics of nanofluids. Bejan introduced a paradigm shift in thermal system optimization methodology through the concept of Entropy Generation Minimization [21]; however, this theoretical framework was not applied to nanofluids, which require a precise balance between heat transfer enhancement and hydraulic effects. On the experimental front, the study by Wen and Ding provided compelling evidence for enhanced heat transfer in nanofluids [22].

The 1998 experimental work by Pak and Cho [23] represents a foundational investigation into nanofluid convection, critically documenting both the attendant thermal enhancement and the consequential rise in viscous dissipation. This study established the enduring paradigm of the thermal-hydraulic trade-off intrinsic to nanofluid systems. The fundamental mechanisms underlying this balance are rooted in classical heat transfer and fluid dynamics principles, as methodically expounded in authoritative references like Nellis and Klein [24], thereby furnishing the theoretical framework requisite for analysing such empirical data.

Based on the comprehensive literature review, a research gap is identified: no prior study has comprehensively considered laminar nanofluid flow with entropy generation in a pipe subjected to a constant heat flux boundary

condition, specifically examining how entropy generation influences the combined thermal and hydraulic performance during the flow and heat transfer process. This study will numerically investigate the laminar flow and heat transfer of an aluminum oxide ($Al_2O_3$) nanofluid, with a nanoparticle diameter of 30 nm and concentrations from 1% to 4%, across a Reynolds number range of 200 to 900. The primary objective is to analyze the effect of nanoparticles on entropy generation and its subsequent impact on the system's thermal and hydraulic performance. $Al_2O_3$/Water was selected for this investigation due to its high thermal efficiency, superior heat transfer characteristics, and relatively low friction factor, which collectively contribute to reducing the required pumping power.

This research establishes its novelty by conducting a thorough analysis of entropy generation in laminar nanofluid flow under a constant heat flux, an area that remains largely unexplored in existing studies. By adopting this entropy-focused methodology, the work provides a fresh thermodynamic viewpoint for evaluating the efficiency of nanofluid-based thermal systems. It directly addresses a known research gap by systematically measuring the concurrent effects of nanoparticle concentration and Reynolds number on entropy generation, Nusselt number, and hydraulic performance, all within a uniform heat flux boundary.

When compared with the results of Hozien et al. [1], Lodhi et al. [2], and Hussien et al. [11], the current investigation corroborates the established trend of improved convective heat transfer with rising nanoparticle concentration. Nonetheless, the specific degree of enhancement observed here differs, attributable to distinct experimental parameters such as particle size, base fluid characteristics, and applied boundary conditions. A key factor that further differentiates this work is its in-depth examination of entropy generation—a component seldom addressed in prior research—thereby defining the unique scope and contribution of this study.

The outcomes of this investigation provide actionable insights for the design and optimization of high-efficiency thermal systems. For design engineers focused on applications such as compact heat exchangers, electronics cooling circuits, or solar thermal absorbers, the results demonstrate that employing $Al_2O_3$-water nanofluid at modest concentrations (1-2%) in conjunction with elevated flow regimes ($Re > 500$) offers considerable advantages. This strategy promotes superior thermal performance by enabling greater heat removal capacity within a fixed volume, thereby allowing for a reduction in the physical size of the system. Concurrently, it elevates thermodynamic efficiency; the observed decrease in total entropy generation indicates a reduction in the destruction of available energy, which can translate into lower operational expenditures over time. The Performance Evaluation Criterion (PEC) and Bejan number further serve as definitive benchmarks for navigating design compromises. A designer might, for example, choose a nanofluid with a high particle concentration to prioritize heat transfer in a severely space-limited setting, accepting the consequent increase in pumping power. Alternatively, a lower concentration could be selected to achieve a more favorable equilibrium between thermal performance and pumping energy consumption.

## 2 Materials and Methods

This research presents a numerical investigation of entropy generation in a laminar, hydrodynamically and thermally developing forced convection of a nanofluid inside a two-dimensional axisymmetric pipe under a constant wall heat flux. The computational analysis was performed using ANSYS Fluent 16.1 to simulate the heat transfer and fluid flow characteristics of an $Al_2O_3$-water nanofluid.

### 2.1 Mathematical Model

The convective flow of a nanofluid within a pipe can be effectively modeled using the Navier-Stokes and energy equations, applying a single-phase approach. Consequently, the governing equations for a two-dimensional, laminar, steady-state, and incompressible flow—assuming a Newtonian fluid with constant thermophysical properties, axisymmetric conditions, and negligible body forces—are as follows [11]:

• Continuity equations:

$$\frac{\partial v_r}{\partial r} + \frac{v_r}{r} + \frac{\partial v_z}{\partial z} = 0 \tag{1}$$

• r-Momentum equation:

$$\rho_{nf}\left(v_r\frac{\partial v_r}{\partial r} + v_z\frac{\partial v_r}{\partial z}\right) = -\frac{\partial p}{\partial r} + \mu_{nf}\left(\frac{\partial}{\partial r}\left(\frac{1}{r}\frac{\partial}{\partial r}\left(rv_r\right)\right) + \frac{\partial^2 v_r}{\partial z^2}\right) \tag{2}$$

• Z-Momentum equation:

$$\rho_{nf}\left(v_r\frac{\partial v_z}{\partial r} + v_z\frac{\partial v_z}{\partial z}\right) = -\frac{\partial p}{\partial z} + \mu_{nf}\left(\frac{1}{r}\frac{\partial}{\partial r}\left(r\frac{\partial v_z}{\partial r}\right) + \frac{\partial^2 v_z}{\partial z^2}\right) \tag{3}$$

• Energy equation:

$$\begin{aligned}\rho_{nf} C_{p_{nf}} \left(v_r \frac{\partial T}{\partial r} + v_z \frac{\partial T}{\partial z}\right) = k_{nf} \left(\frac{1}{r}\frac{\partial}{\partial r}\left(r\frac{\partial T}{\partial r}\right) + \frac{\partial^2 T}{\partial z^2}\right) \\ +\mu_{nf}\left(2\left(\left(\frac{\partial v_r}{\partial z}\right)^2 + \left(\frac{v_r}{r}\right)^2 + \left(\frac{\partial v_z}{\partial z}\right)^2\right) + \left(\frac{\partial v_r}{\partial z} + \frac{\partial v_z}{\partial r}\right)^2\right)\end{aligned} \tag{4}$$

where, $r$, $z$ are radial and axial coordinates, $v_r, v_z$ are radial and axial components of velocity, $\rho_{nf}$ density of nano fluid, $\mu_{nf}$ viscosity of nano fluid, $p$ gage pressure, $T$ absolute temperature, $C_{p_{nf}}$ heat capacity of nano fluid, and $k_{nf}$ thermal conductivity.

Entropy is being generated by two sources: heat transfer and fluid friction.

The general form of the entropy generation equation for pipe geometry is given as [5]:

$$S_{tot} = \frac{(q'')^2 \pi D^2 L}{Nuk_{nf} {T_{avg}}^2} + \frac{32\dot{m}^3 f L}{\pi^2 (\rho_{nf})^2 T_{avg} D^5} \tag{5}$$

where,

$$S_{th} = \frac{(q'')^2 \pi D^2 L}{Nuk_{nf} T_{avg}^2} \tag{6}$$

$$S_{fr} = \frac{32\dot{m}^3 f L}{\pi^2 (\rho_{nf})^2 T_{avg} D^5} \tag{7}$$

$$T_{\text{avg}} = \frac{T_{\text{in}} - T_{\text{out}}}{\ln\left(\frac{T_{\text{in}}}{T_{\text{out}}}\right)} \tag{8}$$

where, $S_{th}$ entropy generated by heat transfer, $S_{fr}$ entropy generated by fluid friction, $S_{tot}$ total entropy generation, $q''$ thermal heat flux, $D$ characteristic dimeter, $L$ pipe length, $Nu$ Nusselt number, $f$ friction coefficient, $T_{avg}$ mean logarithm temperature, $\dot{m}$ mass flow rate.

### 2.2 Models of Nanofluid Properties

A variety of numerical approaches are available for modeling and calculating nanofluid properties. Among these, the single-phase method operates on the fundamental assumption that the nanoparticles and the base fluid are in thermal and dynamic equilibrium, meaning they share identical velocity and temperature fields. This allows the mixture to be treated as a single, homogeneous fluid. Consequently, the standard set of governing equations can be directly applied to this homogeneous medium, requiring only the calculation of its effective thermophysical properties.

• Density

Mixing rule for solid-liquid mixtures were used to find the effective density given as below:

$$\rho_{eff} = (1-\phi)\rho_f + \phi\rho_p \tag{9}$$

where, $\rho_f$ and $\rho_p$ are the base fluid and nanoparticles densities, respectively. $\phi$ is the volume fraction of the nanoparticles.

• Specific heat capacity

The nanofluid specific heat capacity is calculated based on the thermal equilibrium between the base fluid and nanoparticles is given as below:

$$c_{p_{eff}} = \frac{(1-\phi)(\rho c_p)_f + \phi(\rho c_p)_p}{\rho_{eff}} \tag{10}$$

where, $(c_p)_f$ and $(c_p)_p$ are the base fluid and nanoparticles specific heat capacity, respectively.

• Dynamic viscosity

The nanofluid effective dynamic viscosity is determined based on the Masoumi's theoretical model [6]:

$$\mu_{eff} = \mu_f \left( 1 + \frac{\sqrt{\frac{18 K_B \rho_p T}{\pi d_p}}}{72 \mu_f C^3 \sqrt{\frac{\pi}{6\phi}}} \right) \tag{11}$$

where, $K_B$ is Boltzmann constant, $d_p$ is the nanoparticle diameter, and $C$ is the correction factor. While the correction factor is calculated using the following equation:

$$C = \frac{1}{\mu_f}(a\phi + b) \tag{12}$$

where, $a$ = -0.000001133$d_p$-0.000002771, $b$ = 0.00000009$d_p$-0.000000393

• Thermal Conductivity

The nanofluid thermal conductivity effective is defined based on the Vajjha and Das model [7]:

$$k_{\text{eff}} = k_{\text{static}} + k_{\text{Brownian}} \tag{13}$$

$$k_{\text{static}} = \frac{k_p + 2k_f - 2\left(k_f - k_p\right)\phi}{k_p + 2k_f + \left(k_f - k_p\right)\phi} k_f \tag{14}$$

$$k_{\text{Brownian}} = 5 \times 10^4 \beta \phi \left(\rho c_p\right)_f \sqrt{\frac{K_B T}{\rho_p d_p}} f(T, \phi) \tag{15}$$

where, $\beta$ and $f(T, \phi)$ are empirical correlations given as the following:

$$f(T, \phi) = \left(2.8217 * 10^{-2}\phi + 3.917 * 10^{-3}\right)\left(\frac{T}{T_0}\right) + \left(-3.0669 * 10^{-2}\phi - 3.91123 * 10^{-3}\right) \tag{16}$$

where, $T_0$ is the reference temperature which is 273 K. And $\beta$ values for different nanoparticle types are expressed in Table 1.

**Table 1.** Curve-fit $\beta$ relations for $Al_2O_3$ nanoparticles material

| **Nanoparticle** | $\boldsymbol{\beta}$ | $\boldsymbol{\phi}$ | **T(K)** |
|---|---|---|---|
| $Al_2O_3$ | $8.4407(100\phi)^{-1.07304}$ | $1\% \leq \phi \leq 10\%$ | $298\text{K} \leq \text{T} \leq 363\text{K}$ |

Based on the previous equations, the physical properties required for the nanofluid can be calculated. The Table 2 shows the values of the properties of aluminum and water.

**Table 2.** The physical properties of aluminum and water

| **Thermophysical Property** | **Base Fluid (Water)** | **$Al_2O_3$** |
|---|---|---|
| $\rho\left(\frac{kg}{m^3}\right)$ | 996.1 | 3900 |
| $c_p\left(\frac{J}{kg \cdot K}\right)$ | 4072 | 880 |
| $\mu(mPa.s)$ | 0.8538 | – |
| $k\left(\frac{W}{m \cdot K}\right)$ | 0.615 | 35 |

### 2.3 Relevant Dimensionless Numbers

The Reynold number is one of the most important dimensionless numbers. It defines the flow in any region, whether laminar or turbulent, and the formula that expresses the Reynold quantity is:

$$Re = \frac{\rho \overline{v_z} D}{\mu} \tag{17}$$

The friction factor, which is shear at the wall to dynamic pressure, is another significant dimensionless number. The Darcy friction factor can be calculated as follow:

$$f = \frac{-4\tau_w}{0.5\rho \overline{v_z^2}} \tag{18}$$

where,

$$\tau_w = \mu \frac{\partial V_z}{\partial r}\bigg|_{r=R} \tag{19}$$

$$\overline{v_z} = \frac{1}{\pi R^2} \int_0^R v_z(r) 2\pi r dr \tag{20}$$

The Nusselt number is another important dimensionless number defined as the ratio of heat transferred by convection to heat transferred by conduction at the wall. Only when the flow is laminar and in the fully developed region does the Nusselt number remain constant [24].

$$Nu = \frac{hD}{k} \tag{21}$$

where,

$$h = \frac{-K \frac{\partial T}{\partial r}\big|_{r=R}}{\left(T_w - \bar{T}\right)} \tag{22}$$

$$\bar{T} = \frac{\int_0^R v_z T dr}{\int_0^R v_z dr} \tag{23}$$

The Bejan number for entropy generation is the ratio of energy generated due to heat transfer to total entropy generation, with a range of zero to one is given as [9]:

$$Be = \frac{s_{th}}{s_{tot}} \tag{24}$$

Another important parameter is pressure drop (dimensional parameter):

$$\Delta P = \frac{f \overline{v_z^2} L \rho_{nf}}{2DL} \tag{25}$$

The local Nusselt number is calculated along the wall of a micropipe as below in Eq. (21). Where $h$ is a heat transfer coefficient.

The performance criterion represents the enhancement ratio of the heat transfer to the enhancement ratio of the pressure drop as follows:

$$PEC = \frac{\left(\frac{Nu_{nf}}{Nu_{bf}}\right)}{\left(\frac{\Delta P_{nf}}{\Delta P_{bf}}\right)} \tag{26}$$

If PEC $> 1$; the heat transfer performance is higher than the pumping power. That means the system is efficient. If PEC $< 1$; the heat transfer performance is lower than the pumping power. That means the system is not feasible. If PEC = 1; the heat transfer performance is equal to the pumping power. That means the system is not have effectiveness.

### 2.4 Numerical Simulation

The process of numerical modeling encompasses several sequential steps. It begins with the creation of the geometric model, followed by mesh generation. A critical step involves conducting a mesh independence study to ensure the solution is not affected by the grid resolution. Subsequently, the appropriate boundary conditions are defined, and a solution algorithm is selected to guarantee both numerical stability and accelerated convergence. The model's accuracy is then verified, culminating in the post-processing phase where results are extracted, analyzed, and discussed.

• Geometry and boundary conditions

The Figure 1 shows the tube dimensions and boundary conditions used in the numerical analysis. The numerical analysis includes constant values, such as the inlet temperature and heat flux, while the inlet velocity varies in proportion to the Reynolds number and nanoparticle concentration.

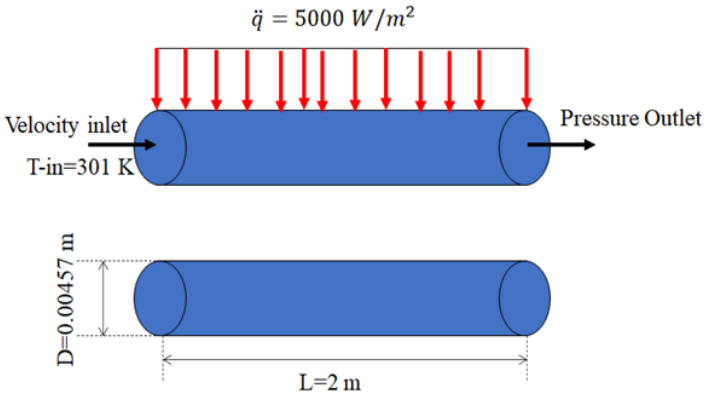


**Figure 1.** Geometry of pipe and boundary conditions

• Mesh independent study

The selection and configuration of the computational mesh are critical to the accuracy of the numerical solution. In this work, a uniformly distributed mesh is applied along the pipe's length, with a refined concentration of elements near the wall. This strategic refinement, achieved through an inflation layer as depicted in Figure 2, is essential for minimizing numerical error and for accurately resolving the steep gradients present within the hydrodynamic and thermal boundary layers.

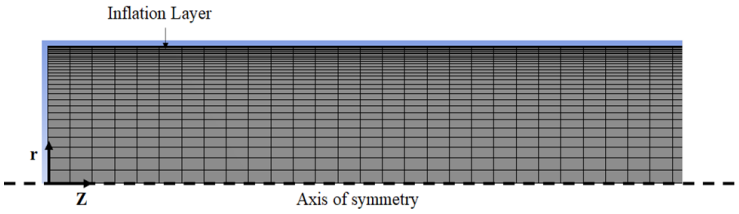


**Figure 2.** Mesh of studied pipe

A structured mesh consisting of quadrilateral cells was implemented to discretize the computational domain. To resolve the pronounced velocity and temperature gradients in the near-wall region, fifteen inflation layers were applied at the boundary. The thickness of the first layer was specifically calibrated to achieve a y+ value below 1.0, ensuring compatibility with the enhanced wall treatment required for the laminar flow model.

A systematic grid refinement process was conducted until the calculated values for the Nusselt number and wall shear stress showed negligible variation. An optimal configuration of 2600 $\times$ 45 cells was identified, achieving an effective compromise between computational accuracy and resource expenditure. This selected mesh density, comprising approximately 117,000 elements, was deemed sufficient as a subsequent refinement to 3000 $\times$ 60 cells altered the Nusselt number by less than 0.1%, confirming that the solution had achieved grid independence.

A mesh independence study was conducted to establish the sufficient cell count in the axial (Z) and radial (r) directions, identifying the point beyond which further grid refinement yields no significant change in the results, thereby ensuring numerical accuracy. This test was performed for pure water at a Reynolds number of 800 across a range of grid densities. The calculated Nusselt number was observed to decrease with increasing cell density until a grid of 2600 $\times$ 45 cells was reached. Beyond this resolution, the results became invariant to additional mesh

refinement. Consequently, a 2600 × 45 grid was selected for all subsequent simulations in this work, as the data in Table 3 confirms it as the optimal cell size.

**Table 3.** Mesh independency test

| Number of Cells in z-Direction | Number of Cells in r-Direction | Nu |
|---|---|---|
| 500 | 10 | 5.434 |
| 1000 | 15 | 5.16 |
| 1500 | 20 | 4.98 |
| 2000 | 25 | 4.88 |
| 2300 | 30 | 4.446 |
| 2600 | 45 | 4.33 |
| 3000 | 60 | 4.33 |

• Solution strategy and validation

In order to solve the required mass conservation, momentum and energy equations, the pseudo-transient algorithm was chosen as a method to velocity-pressure coupling with second order discretization for all equations, the mass conservation equation residuals were adjusted until $10^{-6}$ while energy the equations were allowed to converge until $10^{-10}$.

The validation of numerical results is critical for determining whether our models are correct or not. The numerical values of the Nusselt number along the pipe provided by the fluent solver were compared with the Shah-London [14, 15] correlation in this study.

Shah-London correlation [14, 15]:

$$Nu = 1.302\left(\frac{x^+}{2}\right)^{-\frac{1}{3}} - 0.5, x^+ \leq 0.003 \tag{27}$$

$$Nu = 4.364 + 0.263\left(\frac{x^+}{2}\right)^{-0.506} e^{-41\left(x^+/2\right)}, \quad x^+ > 0.003 \tag{28}$$

where, $x^+ = \frac{2(x/D)}{\mathrm{RePr}}$.

Figure 3 shows that there is a very good agreement between the Shah-London correlation and the current results. These results are obtained for pure water at Re = 800.

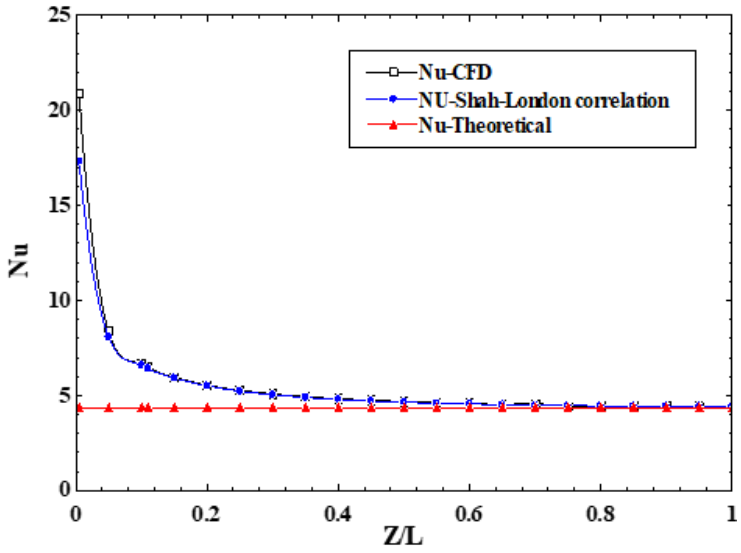


**Figure 3.** Nusselt number along the pipe calculated numerically compared with the Shah-London correlation

## 3 Results and Discussions

This study aims to investigate entropy generation and the convective heat transfer coefficient for nanofluid flow within a two-dimensional pipe. The pipe wall is subjected to a uniform heat flux of 5000 W/m$^2$. The inlet velocity is defined by the Reynolds number, which varies from 200 to 900, with a constant inlet temperature of 301 K. The working fluid is an $Al_2O_3$-water nanofluid with nanoparticle volume concentrations from 1% to 4% in 1% increments and a consistent nanoparticle diameter of 30 nm. The thermophysical properties of the nanofluid are determined using a single-phase model that incorporates the effects of Brownian motion and nanoparticle diameter.

The influence of nanoparticle concentration on velocity profiles is illustrated in Figure 4 for a Reynolds number of 800. The contour plot reveals that the highest axial velocity occurs at the maximum volume concentration of 4%. This phenomenon is attributed to the increase in both viscosity and density that accompanies a higher nanoparticle load. Since the Reynolds number is held constant, the ratio of these properties adjusts, leading to an elevated centerline velocity with increasing concentration ($\varphi$). Furthermore, the velocity profile demonstrates a characteristic distribution: it reaches a minimum at the pipe wall due to viscous friction and a maximum at the centerline. This pattern is accentuated by the favorable mixing between fluid layers and solid nanoparticles, which enhances the inertial forces within the flow.

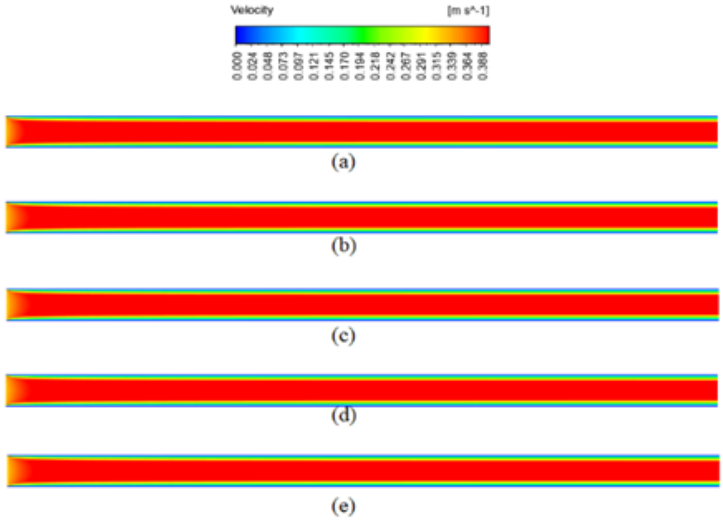


**Figure 4.** Velocity contours at $d_p$ = 30 and Re=800: (a) pure water; (b) 1% volume concentrations; (c) 2% volume concentrations; (d) 3% volume concentrations; and (e) 4% volume concentrations

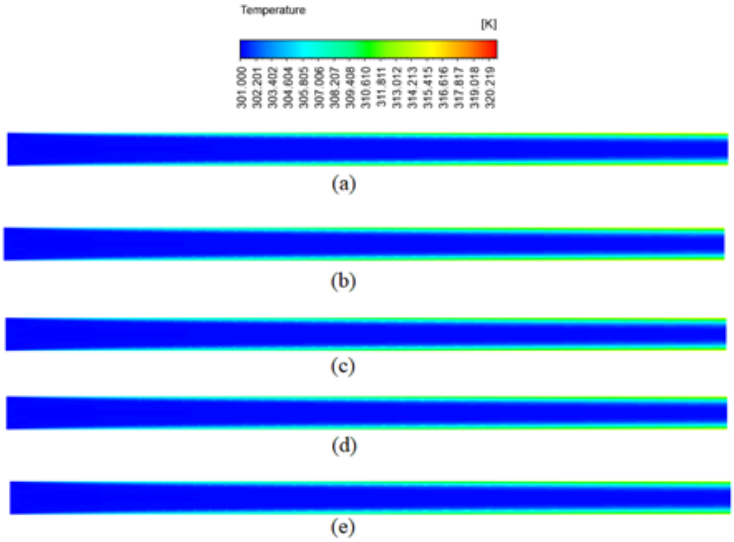


**Figure 5.** Temperature contours Re = 800, $d_p$ = 30 nm: (a) pure water; (b) 1% volume concentrations; (c) 2% volume concentrations; (d) 3% volume concentrations; and (e) 4% volume concetrations

The observed rise in maximum velocity alongside increasing nanoparticle concentration, under a constant Reynolds number, is a direct outcome of the Reynolds number's definition ($\mathrm{Re} = \rho \mathrm{x} \mathrm{D}/\mu$). At higher concentrations ($\varphi$), the nanofluid's density ($\rho$) and dynamic viscosity ($\mu$) both rise; however, the relative increase in viscosity is more pronounced. To maintain a specified Reynolds number, the inlet velocity ($v$) must therefore be raised, leading to the higher velocity magnitudes visible in the contour plots.

Figure 5 illustrates the temperature contours along the pipe's length. The contours reveal a clear thermal gradient, with temperature varying both axially from the inlet to the outlet and radially from the centerline to the wall. The minimum temperature is located at the centerline of the inlet section, while the maximum temperature occurs at the wall of the outlet cross-section.

Pressure contours are presented in Figure 6, illustrating the progressive pressure drop along the flow direction, which constitutes the primary driving force for the fluid. The data indicates that a higher nanoparticle concentration results in a more significant pressure loss. This phenomenon is attributed to increased flow resistance, stemming from greater obstruction to fluid movement and elevated density associated with the nanofluid.

The accelerated pressure decline observed with rising volume concentration ($\varphi$) results from two interrelated factors. First, the enhanced nanofluid viscosity amplifies wall shear stress. Second, the requisite increase in inlet velocity to maintain a constant Reynolds number elevates the flow's dynamic head, thereby intensifying frictional losses. This graphical data provides clear visual confirmation of the increased pumping power necessary at elevated nanoparticle concentrations.

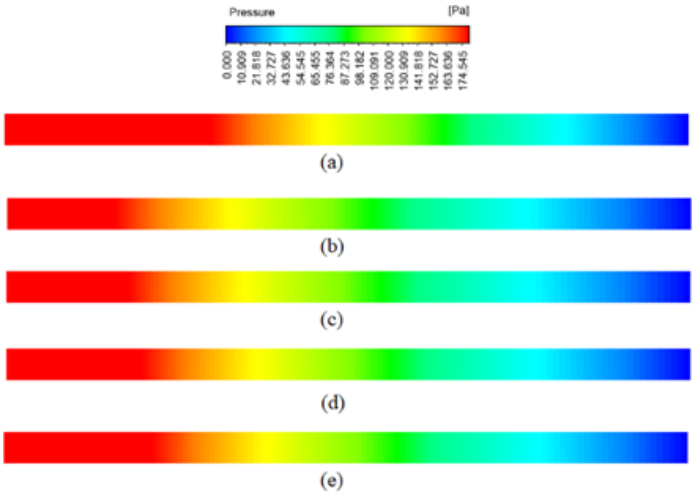


**Figure 6.** Pressure contours Re = 800, $d_p$ = 30 nm: (a) pure water; (b) 1% volume concentrations; (c) 2% volume concentrations; (d) 3% volume concentrations; and (e) 4% volume concentrations

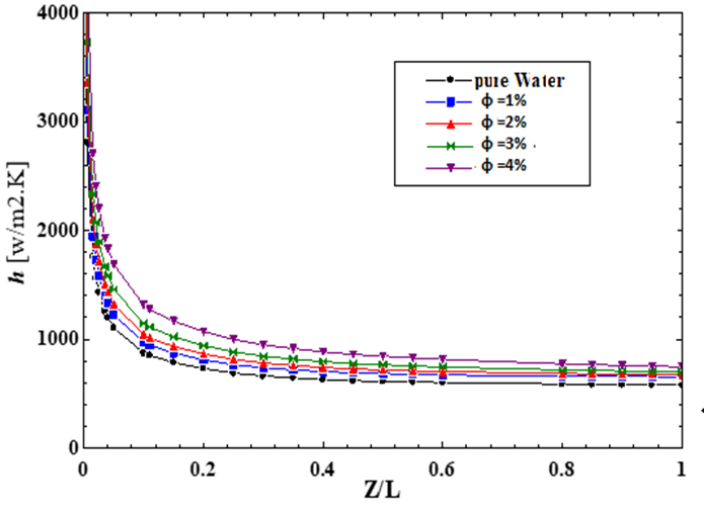


**Figure 7.** The effect of nanoparticles concentrations versus axial locations on HTC at Re = 800 and $d_p$ = 30 nm

The influence of nanoparticle concentration on the heat transfer coefficient (HTC) and Nusselt number along the pipe's axial direction is presented in Figure 7 and Figure 8. The HTC demonstrates a clear enhancement with rising nanofluid volume concentration. This improvement is driven by a reduction in the temperature difference between the pipe wall and the fluid's mean temperature, as visually confirmed in Figure 7. Consequently, the incorporation of nanoparticles directly augments the convective heat transfer performance. A corresponding increase in the Nusselt number with higher concentrations is also evident in Figure 8. This trend is expected, as a greater volume fraction of nanoparticles elevates the effective thermal conductivity of the fluid, thereby promoting more efficient heat transfer.

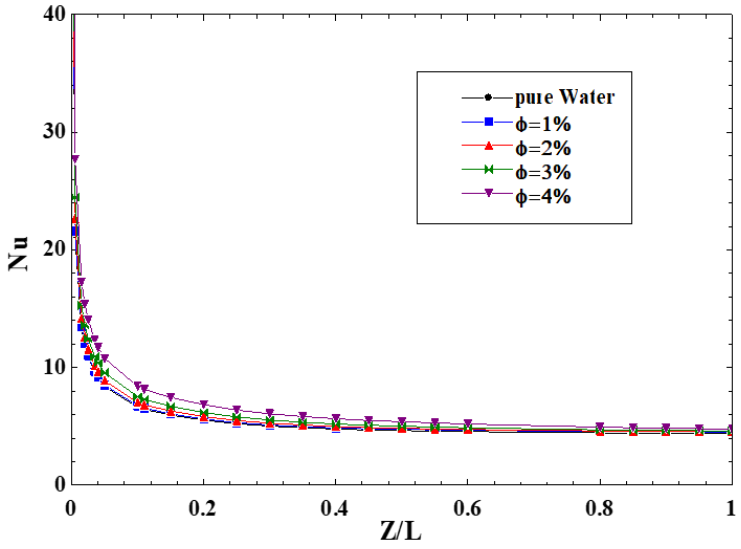


**Figure 8.** The effect of nanoparticles concentrations versus axial locations on Nusselt number at Re = 800 and $d_p$ = 30 nm

Figure 9 illustrates the combined influence of nanoparticle volume concentration and Reynolds number on the average Nusselt number. This enhancement stems from improved mixing within the fluid layers, favorable inertial forces, and the fundamental improvement in the nanofluid's thermal conductivity coupled with its reduced specific heat capacity, which lowers its energy storage potential. The results confirm that the average Nusselt number rises with both increasing volume fraction and Reynolds number. A maximum augmentation of 27.07% in the average Nusselt number was achieved under the conditions of a 30 nm particle diameter, a Reynolds number of 900, and a volume concentration ($\varphi$) of 4%.

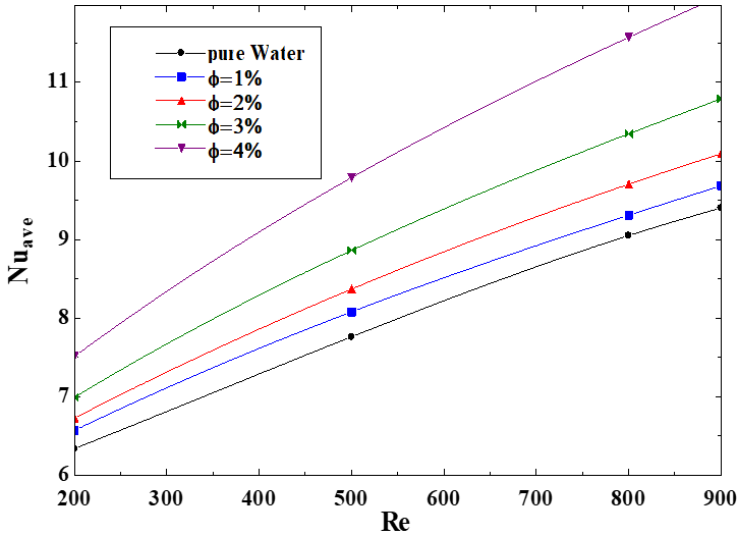


**Figure 9.** Variation of the average Nusselt number with Re, $\varphi$ at $d_p$ = 30 nm

The relationship between Reynolds number (Re) and wall shear stress across various volume concentrations ($\varphi$) is shown in Figure 10. For a fixed $\varphi$, the shear stress rises with increasing Re. This occurs because a higher flow velocity

intensifies the velocity gradient within the wall region, thereby elevating the shear stress. Conversely, at a constant Re, the shear stress exhibits a non-linear increase with $\varphi$. This trend is attributed to the higher nanoparticle count at elevated concentrations, which augments the nanofluid's viscosity. The analysis also reveals that the influence of $\varphi$ on shear stress is minimal at low Reynolds numbers, remaining negligible up to $\varphi$ = 0.02. In contrast, the effect of nanoparticle concentration becomes markedly more pronounced at Reynolds numbers up to 300.

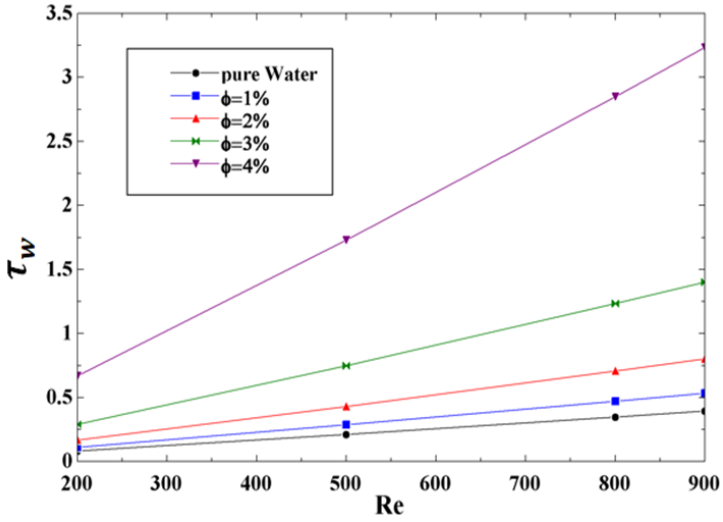


**Figure 10.** The effect of Re, $\varphi$ on the wall shear stress at $d_p$ = 30 nm

Figure 11 demonstrates the influence of Reynolds number on the thermal entropy generation across different nanoparticle volume fractions ($\varphi$). The data shows that for a constant $\varphi$, thermal entropy generation decreases with increasing Re. This reduction occurs because higher flow velocities intensify fluid mixing, which enhances heat transfer efficiency and consequently diminishes irreversibilities. Additionally, at any fixed Reynolds number, thermal entropy generation declines as $\varphi$ increases. This trend is logical, since a higher nanoparticle concentration improves the effective thermal conductivity, thereby facilitating more efficient heat exchange between the wall and the fluid. This enhanced heat transfer reduces the temperature gradient between the wall and the core flow, leading to lower entropy generation.

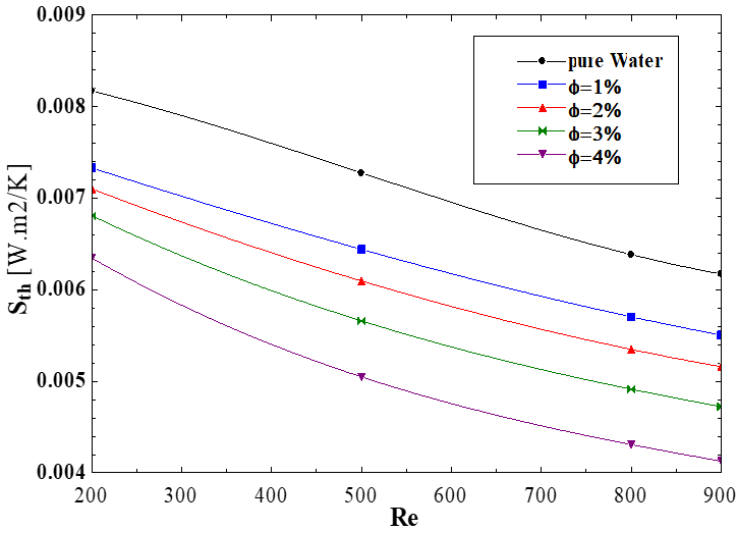


**Figure 11.** The effect of Re and $\varphi$ on the thermal entropy generation at $d_p$ = 30 nm

Figure 12 illustrates the relationship between Reynolds number and frictional entropy generation for different volume fractions ($\varphi$). The data reveals a nonlinear rise in frictional entropy generation with increasing nanoparticle concentration at any constant Re. This trend is a direct consequence of the accompanying increase in nanofluid viscosity. The impact of nanoparticle concentration is marginal for $\varphi \leq 0.02$ but becomes substantial at higher values.

Meanwhile, Figure 13 presents the combined effect of Re and $\varphi$ on the total entropy generation. The overall trend demonstrates that increasing the Reynolds number reduces the total entropy generation. By comparing Figure 11 and Figure 12, it is evident that the reduction in thermal entropy outweighs the concurrent increase in frictional entropy. This net effect accounts for the overall decline in total entropy generation with higher Re. The maximum observed reduction in total entropy generation was 22.25%, which occurred for a particle diameter of 30 nm at Re = 900 when the volume fraction was increased from $\varphi$ = 0 (pure water) to $\varphi$ = 0.04.

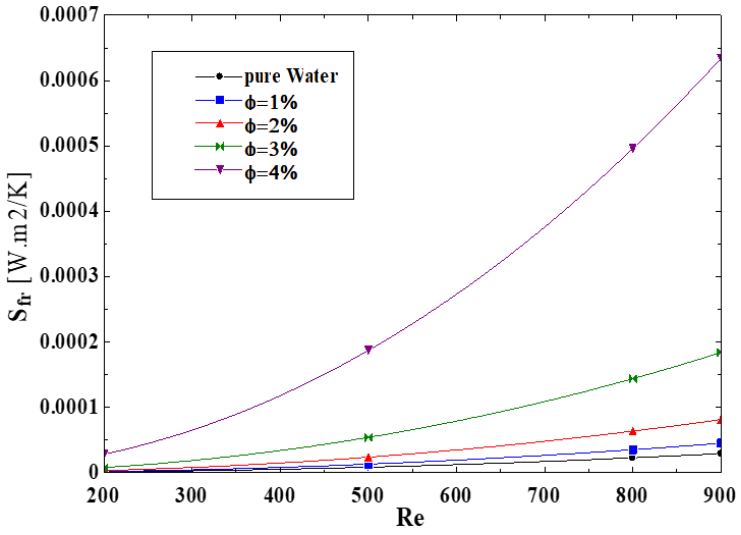


**Figure 12.** The effect of Re and $\varphi$ on the friction entropy generation at $d_p$ = 30 nm

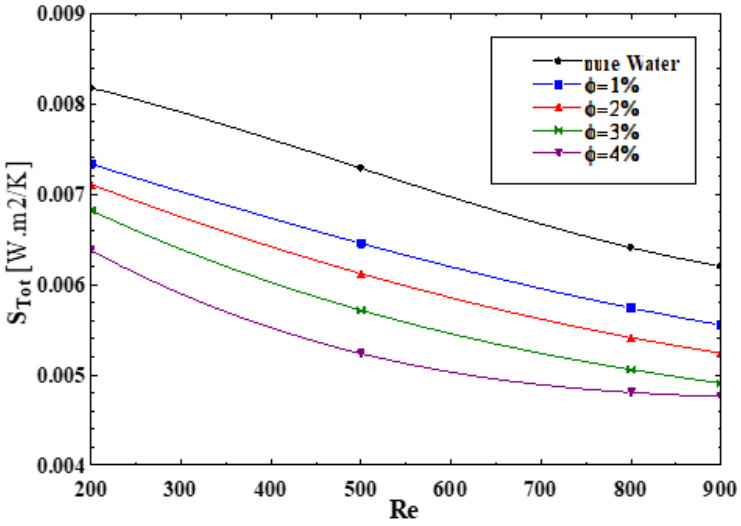


**Figure 13.** The effect of Re and $\varphi$ on the total entropy generation at $d_p$ = 30 nm

The overall influence of the Reynolds number on the Bejan number can be readily interpreted by considering the interplay between thermal and frictional entropy generation, as detailed in the preceding analysis. Figure 14 demonstrates that an increase in Reynolds number leads to a reduction in the Bejan number, with this effect becoming more pronounced at higher Reynolds numbers and nanoparticle volume fractions. However, the impact of Reynolds number on Bejan number remains nearly negligible for volume fractions up to 0.02.

Figure 15 illustrates the impact of the nanoparticle volume fraction ($\varphi$) on the Performance Evaluation Criterion (PEC). A PEC value exceeding unity indicates a beneficial use of nanofluid, as the relative enhancement in heat transfer outweighs the relative increase in pumping power due to pressure drop. Conversely, a value below one suggests that the penalty of increased pumping power surpasses the thermal benefit. For the specific nanofluid analyzed in this research, elevating the nanoparticle concentration demonstrated a negative effect on the PEC. However, it is crucial to note that while higher $\varphi$ values demanded greater pumping power, they also contributed to a significant reduction in total entropy generation, representing a key thermodynamic advantage.

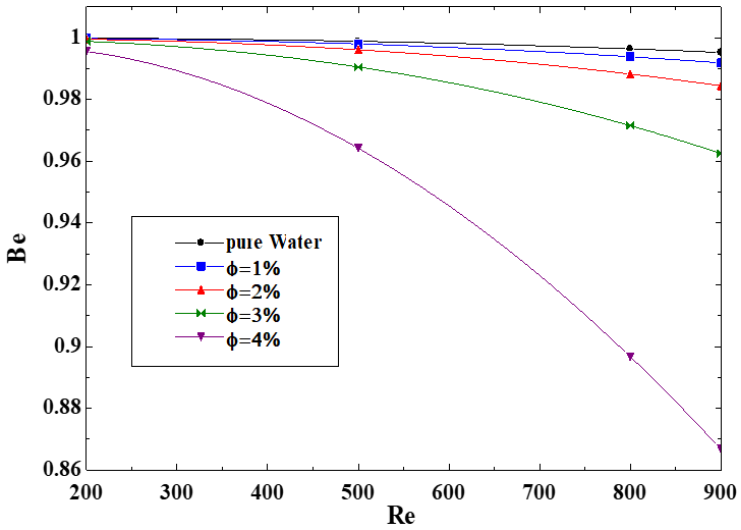


**Figure 14.** The effect of Re and $\varphi$ on Be at $d_p$ = 30 nm

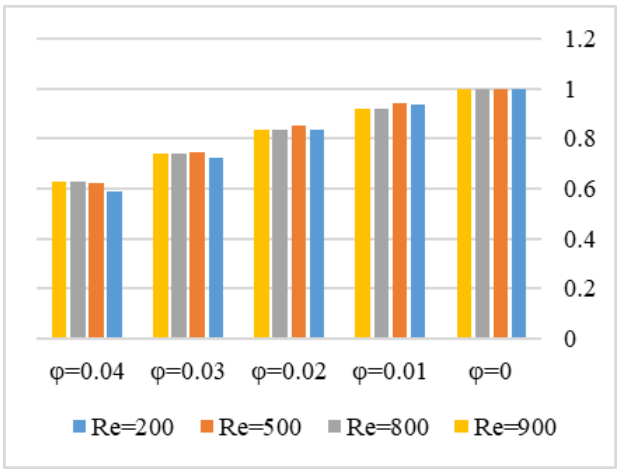


**Figure 15.** The PEC of nanofluids with different values of $\varphi$ and Re at $d_p$ = 30 nm

From a physical standpoint, the pressure drop along the pipe axis results from the combined mechanisms of viscous dissipation and momentum diffusion. Elevated nanoparticle concentrations exacerbate this pressure loss due to the accompanying rise in the nanofluid's density and viscosity, which collectively amplify the resistance to flow. This behavior underscores a critical design trade-off: the thermal performance gains achieved through nanoparticles are accompanied by a non-negligible hydraulic penalty that must be considered in practical system design.

The findings reveal a pronounced sensitivity of the system's performance to variations in both the Reynolds number and nanoparticle concentration. A strong, positive correlation is observed between the average Nusselt number and increases in either parameter. Of particular significance is the high sensitivity of total entropy generation to the Reynolds number, which exhibits a substantial decline as Re increases. The relationship with volume concentration ($\varphi$) is non-linear; its influence on frictional entropy generation intensifies considerably beyond a threshold of $\varphi = 2\%$. This non-linearity suggests that operating with volume concentrations below 2% can provide the desired heat transfer enhancement while avoiding excessive penalties in pumping power and frictional irreversibility.

## 4 Conclusion

This numerical investigation confirms that employing $Al_2O_3$-water nanofluid in laminar pipe flow under a constant heat flux boundary condition offers a dual advantage: simultaneous enhancement of heat transfer rates and a reduction in thermodynamic irreversibility. A primary practical finding is that system efficiency is optimized at higher Reynolds numbers coupled with lower nanoparticle concentrations, specifically within the 1–2% range. This operational regime achieves a significant thermal performance improvement of up to 27% alongside a substantial 22% reduction in total entropy generation, indicating a more efficient system with lower energy waste. For design scenarios where pumping power is a major constraint, the Performance Evaluation Criterion (PEC) serves as the

essential design metric. Conversely, in applications demanding maximum heat dissipation, higher nanoparticle concentrations may be justified, provided the associated increase in frictional entropy is acknowledged.

This investigation numerically analyzes entropy generation for $Al_2O_3$-water nanofluid flow in a two-dimensional axisymmetric pipe, with viscous dissipation incorporated into the model. A single-phase approach is employed to simulate the nanofluid's flow and convective heat transfer characteristics. The research systematically examines the influence of key governing parameters: nanoparticle volume concentration, Reynolds number, and nanoparticle size. The findings derived from the analysis lead to the following conclusions:

• Elevating the nanoparticle concentration leads to an increase in the flow's maximum velocity, overall pressure drop, and wall shear stress.

• A higher nanoparticle concentration reduces the temperature difference between the pipe wall and the bulk fluid, resulting in a concomitant rise in both the heat transfer coefficient and the Nusselt number. The peak enhancement of 27.07% in the average Nusselt number was observed at Re = 900, $\varphi$ = 0.04, and with a particle diameter ($d_p$) of 30 nm.

• Increasing the nanoparticle concentration reduces the thermal component of entropy generation but augments the frictional component. The net effect is a decrease in both the total entropy generation and the Bejan number. The maximum recorded reduction in total entropy generation was 22.25% for the conditions of Re = 900, $\varphi$ = 0.04, and $d_p$ = 30 nm.

This study is limited by the use of a single-phase numerical approach, which assumes uniform thermal equilibrium between the base fluid and nanoparticles. Future investigations should implement two-phase or Eulerian–Lagrangian models to capture slip velocity and particle migration effects. Additionally, experimental validation is recommended to confirm numerical predictions and extend the analysis to turbulent regimes and other nanoparticle types.

## Data Availability

The data used to support the findings of this study are available from the corresponding author upon request.

## Conflicts of Interest

The authors declare that they have no conflicts of interest.

## References


[1] O. Hozien, W. El-Maghlany, M. Sorour, and Y. Mohamed, "Experimental study on heat transfer and pressure drop characteristics utilizing three types of water based nanofluids in a helical coil under isothermal boundary condition," *J. Taiwan Inst. Chem. Eng.*, vol. 128, pp. 237–252, 2021. https://doi.org/10.1016/j.jtice.2021.08.028

[2] M. S. Lodhi, T. Sheorey, and G. Dutta, "Single-phase fluid flow and heat transfer characteristics of nanofluid in a circular microchannel: Development of flow and heat transfer correlations," *Proc. Inst. Mech. Eng. Part C J. Mech. Eng. Sci.*, vol. 234, no. 18, pp. 3689–3708, 2020. https://doi.org/10.1177/0954406220916537

[3] S. A. Adio, A. O. Muritala, A. S. Binuyo, T. Oketola, and V. R. Veeredhi, "Eulerian multiphase technique for detailed investigation on hydro-thermal enhancement in a cooling microchannel using pulsating alumina nanofluid: A numerical simulation," *Case Stud. Therm. Eng.*, vol. 59, p. 104482, 2024. https://doi.org/10.1016/j.csite.2024.104482

[4] Z. Alhajaj, A. M. Bayomy, and M. Z. Saghir, "A comparative study on best configuration for heat enhancement using nanofluid," *Int. J. Thermofluids*, vol. 7, p. 100041, 2020. https://doi.org/10.1016/j.ijft.2020.100041

[5] H. Herwig and O. Hausner, "Critical view on 'new results in micro-fluid mechanics': An example," *Int. J. Heat Mass Transf.*, vol. 46, no. 5, pp. 935–937, 2003. https://doi.org/10.1016/S0017-9310(02)00306-X

[6] N. Masoumi, N. Sohrabi, and A. Behzadmehr, "A new model for calculating the effective viscosity of nanofluids," *J. Phys. D: Appl. Phys.*, vol. 42, no. 5, p. 055501, 2009. https://doi.org/10.1088/0022-3727/42/5/055501

[7] R. S. Vajjha and D. K. Das, "Experimental determination of thermal conductivity of three nanofluids and development of new correlations," *Int. J. Heat Mass Transf.*, vol. 52, no. 21–22, pp. 4675–4682, 2009. https://doi.org/10.1016/j.ijheatmasstransfer.2009.06.027

[8] T. L. Bergman, A. S. Lavine, F. P. Incropera, and D. P. DeWitt, *Fundamentals of Heat and Mass Transfer*, 7th ed. John Wiley & Sons, 2016.

[9] T. F. J. Irvine and J. P. Hartnett, Eds., *Advances in Heat Transfer*. Volume 1, Academic Press, 1946.

[10] M. Kalteh, A. Abbassi, M. Saffar-Avval, A. Frijns, A. Darhuber, and J. Harting, "Experimental and numerical investigation of nanofluid forced convection inside a wide microchannel heat sink," *Appl. Therm. Eng.*, vol. 36, pp. 260–268, 2012. https://doi.org/10.1016/j.applthermaleng.2011.10.023

[11] A. A. Hussien, M. Z. Abdullah, N. M. Yusop, W. Al-Kouz, E. Mahmoudi, and M. Mehrali, "Heat transfer and entropy generation abilities of MWCNTs/GNPs hybrid nanofluids in microtubes," *Entropy*, vol. 21, no. 5, p. 480, 2019. https://doi.org/10.3390/e21050480

[12] M. M. Heyhat, F. Kowsary, A. M. Rashidi, M. H. Momenpour, and A. Amrollahi, "Experimental investigation of laminar convective heat transfer and pressure drop of water-based $Al_2O_3$ nanofluids in fully developed flow regime," *Exp. Therm. Fluid Sci.*, vol. 44, pp. 483–489, 2013. https://doi.org/10.1016/j.expthermflusci.2012.08.009

[13] K. S. Hwang, S. P. Jang, and S. U. Choi, "Flow and convective heat transfer characteristics of water-based $Al_2O_3$ nanofluids in fully developed laminar flow regime," *Int. J. Heat Mass Transf.*, vol. 52, no. 1–2, pp. 193–199, 2009. https://doi.org/10.1016/j.ijheatmasstransfer.2008.06.032

[14] R. K. Shah and A. L. London, *Laminar Flow Forced Convection in Ducts: Supplement 1 to Advances in Heat Transfer*. Academic Press, 1978.

[15] R. K. Shah and M. S. Bhatti, "Chapter 3: Laminar convective heat transfer in ducts," in *Handbook of Single-Phase Convective Heat Transfer*. John Wiley & Sons, 1987.

[16] V. Anand, "Entropy generation analysis of laminar flow of a nanofluid in a circular tube immersed in an isothermal external fluid," *Energy*, vol. 93, pp. 154–164, 2015. https://doi.org/10.1016/j.energy.2015.09.019

[17] B. H. Salman, H. A. Mohammed, K. M. Munisamy, and A. S. Kherbeet, "Three-dimensional numerical investigation of nanofluids flow in microtube with different values of heat flux," *Heat Transf. Asian Res.*, vol. 44, no. 7, pp. 599–619, 2015. https://doi.org/10.1002/htj.21139

[18] H. H. Ting and S. S. Hou, "Numerical study of laminar flow forced convection of water-$Al_2O_3$ nanofluids under constant wall temperature condition," *Math. Probl. Eng.*, vol. 2015, no. 1, p. 180841, 2015. https://doi.org/10.1155/2015/180841

[19] S. X. Zhang, Y. L. He, G. Lauriat, and W. Q. Tao, "Numerical studies of simultaneously developing laminar flow and heat transfer in microtubes with thick wall and constant outside wall temperature," *Int. J. Heat Mass Transf.*, vol. 53, no. 19–20, pp. 3977–3989, 2010. https://doi.org/10.1016/j.ijheatmasstransfer.2010.05.017

[20] M. H. Fard, M. N. Esfahany, and M. R. Talaie, "Numerical study of convective heat transfer of nanofluids in a circular tube two-phase model versus single-phase model," *Int. Commun. Heat Mass Transf.*, vol. 37, no. 1, pp. 91–97, 2010. https://doi.org/10.1016/j.icheatmasstransfer.2009.08.003

[21] A. Bejan, *Entropy Generation Minimization: The Method of Thermodynamic Optimization of Finite-Size Systems and Finite-Time Processes*. CRC Press, 1995.

[22] D. Wen and Y. Ding, "Experimental investigation into convective heat transfer of nanofluids at the entrance region under laminar flow conditions," *Int. J. Heat Mass Transf.*, vol. 47, no. 24, pp. 5181–5188, 2004. https://doi.org/10.1016/j.ijheatmasstransfer.2004.07.012

[23] B. C. Pak and Y. I. Cho, "Hydrodynamic and heat transfer study of dispersed fluids with submicron metallic oxide particles," *Exp. Heat Transf.*, vol. 11, no. 2, pp. 151–170, 1998. https://doi.org/10.1080/08916159808946559

[24] G. Nellis and S. Klein, *Heat Transfer*. Cambridge University Press, 2008.

**Nomenclature**

| | |
|---|---|
| Be | Bejan number |
| $C_p$ | Specific heat, J·kg$^{-1}$·K$^{-1}$ |
| D | Pipe diameter, m |
| h | Convection heat transfer coefficient, W·m$^{-2}$·K$^{-1}$ |
| K | Thermal conductivity, W·m$^{-1}$·K$^{-1}$ |
| Nu | Nusselt number |
| P | Pressure, Pa |
| Re | Reynolds number |
| $r$, $z$ | Cylindrical coordinates |
| S | Entropy generation |
| T | Temperature, K |
| $v_r$, $v_z$ | Velocity components in $r$ and $z$ directions, m·s$^{-1}$ |

Greek symbols

| | |
|---|---|
| $\alpha$ | Thermal diffusivity, m$^2$· s$^{-1}$ |
| $\beta$ | Thermal expansion coefficient, K$^{-1}$ |
| $\phi$ | Solid volume fraction |
| $\rho$ | Density, kg· m$^{-3}$ |
| $\mu$ | Dynamic viscosity, kg· m$^{-1}$· s$^{-1}$ |

Subscripts

| | |
|---|---|
| Avg | Average |
| bf | Base fluid |
| Eff | Effective |
| f | Pure fluid |
| nf | Nanofluid |
| np | Nanoparticle |